

---

# Wakes in Dark Matter Halos

Burkhard Fuchs

Astronomisches Rechen-Institut, Mönchhofstr. 12-14, 69120 Heidelberg, Germany  
[fuchs@ari.uni-heidelberg.de](mailto:fuchs@ari.uni-heidelberg.de)

**Summary.** I discuss the dynamical interaction of galactic disks with the surrounding dark matter halos. In particular it is demonstrated that if the self-gravitating shearing sheet, a model of a patch of a galactic disk, is embedded in a live dark halo, this has a strong effect on the dynamics of density waves in the sheet. I describe how the density waves and the halo interact via halo particles either on orbits in resonance with the wave or on non-resonant orbits. Contrary to expectation the presence of the halo leads to a very considerable enhancement of the amplitudes of the density waves in the shearing sheet. This effect appears to be the equivalent of the recently reported enhanced growth of bars in numerically simulated stellar disks embedded in live dark halos. Finally I discuss the counterparts of the perturbations of the disk in the dark halo.

## 1 Introduction

Dark halos are usually thought to stabilize galactic disks against non-axisymmetric instabilities. This was first proposed by Ostriker & Peebles (1973) on the basis of – low-resolution – numerical simulations. Their physical argument was that the presence of a dark halo reduces the destabilizing self-gravity of the disks. Doubts about an entirely passive role of dark halos were raised by Toomre (1977), but he (Toomre 1981) also pointed out that a dense core of a dark halo may cut the feed-back loop of the corotation amplifier of bars or spiral density waves and suppress thus their growth. Recent high-resolution numerical simulations by Athanassoula (2002, 2003), also inherent in the work of Debatista & Sellwood (2000), have shown that quite the reverse, a *destabilization* of disks immersed in dark halos, might be actually true. Athanassoula (2002) demonstrated clearly that much stronger bars grow in the simulations if the disk is embedded in a live dark halo instead of a static halo potential. This is attributed to angular momentum transfer from the bar to the halo via halo particles on resonant orbits. Angular momentum exchange between disk and halo has been addressed since the pioneering work of Weinberg (1985) in many studies theoretically or by numerical simulations and I refer to Athanassoula

(2003) for an overview of the literature. Toomre (1981) has shown how the bar instability can be understood as an interference of spiral density waves in a resonance cavity between the corotation amplifier and an inner reflector (cf. also Fuchs 2004b). Thus it is to be expected that a live dark halo will be also responsive to spiral density waves and develop wakes. That this is indeed the case has been demonstrated by Fuchs (2004a) employing the shearing sheet model. This adds to the confidence in the results of the numerical work on bar growth in galactic disks.

The shearing sheet (Goldreich & Lynden-Bell 1965, Julian & Toomre 1966) model has been developed as a tool to study the dynamics of galactic disks and is particularly well suited to describe theoretically the dynamical mechanisms responsible for the formation of spiral arms. For the sake of simplicity the model describes only the dynamics of a patch of a galactic disk. It is assumed to be infinitesimally thin and its radial size is assumed to be much smaller than the disk. Polar coordinates can be therefore rectified to pseudo-Cartesian coordinates and the velocity field of the differential rotation of the disk can be approximated by a linear shear flow. These simplifications allow an analytical treatment of the problem, which helps also in the present case to clarify the underlying physical processes operating in the disk.

## 2 Shearing sheet model

The basic disk model is the stellardynamical shearing sheet, which describes the local dynamics of a patch of a thin, differentially rotating stellar disk. Stellar orbits are calculated in a frame at a distance  $r_0$  from the galactic center, rotating with an angular velocity  $\Omega_0$ . Pseudo-Cartesian coordinates  $x$  and  $y$  point in the radial direction and tangential to the direction of galactic rotation, respectively. The differential rotation of the disk is approximated as a parallel shear flow,  $v = -2Ax$ , with  $A$  denoting Oort's constant. The surface density  $\Sigma_0$  is assumed to be constant over the entire region. As is well known (cf. Julian & Toomre 1966) the stellar orbits in this model are simply epicyclic orbits and the phase space distribution function of the stars  $f_0$ , as derived from the time-independent Boltzmann-equation, is a Schwarzschild-distribution. A cartoon of the shearing sheet model is shown in Fig. 1.

**Fig. 1.** The shearing sheet model

The disk is subjected to potential perturbations

$$\delta\Phi = \int d\omega \int dk_x \int dk_y \Phi_{\mathbf{k},\omega} e^{i(\omega t + k_x x + k_y y)}, \quad (1)$$

and the response of the disk,  $f_1$ , is calculated from the linearized Boltzmann-equation

$$\frac{\partial f_1}{\partial t} + [f_0, \delta\Phi] + [f_1, H_0] = 0, \quad (2)$$

written in general form with Poisson brackets.  $H_0$  denotes the Hamiltonian of the stellar orbits in the unperturbed disk. In order to obtain self-consistent perturbations the response density has to be inserted into the Poisson-equation

$$\Delta\delta\Phi = 4\pi G \int d^2v f_1, \quad (3)$$

where  $G$  is the constant of gravitation. Unfortunately, the disk response to a single Fourier component of the potential perturbation (1) is not a Fourier component of the general disk response. I follow therefore Kalnajs (1971) and take scalar products,

$$\frac{1}{4\pi^2} \int dx \int dy e^{-i(k'_{xx} + k'_{yy})} \dots, \quad (4)$$

of both sides of the Poisson-equation with conjugate basis functions of the Fourier transform. Details of the evaluation of the quadratures, which are carried out using action and angle variables are given in (Fuchs 2001). The result is that the Poisson-equation is converted to an integral equation of Volterra-type, which is equivalent to the integral equation given by Julian & Toomre (1966), although it is not formulated in shearing coordinates,

$$\Phi_{\mathbf{k}',\omega} = \int_{-\infty}^{k'_x} dk_x \mathcal{K}(k_x, k'_x, k'_y, \omega) \Phi_{k_x, k'_y, \omega}, \quad (5)$$

with a kernel  $\mathcal{K}$  that can be expressed analytically (Fuchs 2001)<sup>1</sup>. By Fredholm discretization equation (5) can be transformed into a set of algebraic equations. The kernel  $\mathcal{K}$  vanishes on the diagonal, so that the triangular coefficient matrix of this set of equations has an unity diagonal, implying a non-vanishing determinant. Thus the homogenous integral equation (5) has no eigensolutions, indicating that there exist in the shearing sheet no – except ringlike ( $k'_y = 0$ ) – proper spiral modes in the sense of rigidly rotating spatial patterns with well defined growth rates. External potential perturbations or initial ( $t = 0$ ) density or velocity perturbations of the basic state of the disk are represented by an inhomogeneous term in the integral equation (5), or the corresponding integral equation for the surface density

$$\Sigma_{\mathbf{k}',\omega} = \int_{-\infty}^{k'_x} dk_x \mathcal{K}(k_x, k'_x, k'_y, \omega) \Sigma_{k_x, k'_y, \omega} + r_{\mathbf{k}',\omega}. \quad (6)$$

The resolvent kernel  $\mathcal{R}(k_x, k'_x, k'_y, \omega)$  of the inhomogeneous integral equation (6) can be obtained as a Neumann series. Solutions of equation (6) are then found in a unique way by a convolution of  $\mathcal{R}$  with the inhomogeneous terms

---

<sup>1</sup> Positive wave numbers  $k'_y$  will be assumed in the following.

$r_{\mathbf{k}'}$ . Transforming these solutions back from  $\omega$ - to time-domain one can show that the resulting spatial pattern is a superposition of ‘swinging’ density waves, shearing with the general flow, but exhibiting transient growth as they swing by until they finally decay. Fig. 2, taken from Fuchs (1991), illustrates this for single plane sinusoidal waves,  $r_{\mathbf{k}'} \propto \delta(k'_x - k_x^{in})$ , all of the same initial radial wave number  $k_x^{in}$ . The resulting spatial pattern evolves then as

**Fig. 2.** Amplitudes of swing amplified density waves with initial radial wave numbers  $k_x^{in} = -1$  (leading waves). Wave numbers are given in units of  $k_{\text{crit}} = \kappa^2 / 2\pi G \Sigma_0$ , where  $\kappa$  denotes the epicyclic frequency. Time is in units of  $(2Ak_y)^{-1}$ . The Toomre stability parameter is  $Q = 1.4$ , and an Oort constant of  $A = \Omega_0/2$  is assumed.

$$\Sigma(x, y, t) = \delta(t) e^{i(k_x^{in}x + k'_y y)} + \tilde{\mathcal{R}}(k_x^{in}, k_x^{in} + 2Ak'_y t) e^{i[(k_x^{in} + 2Ak'_y t)x + k'_y y]}, \quad (7)$$

where the swinging around of the wave crests of the density waves is described by the growth of the effective radial wave number  $k_x^{in} + 2Ak'_y t$  with time. As is well known, amplification is high for density waves, which are initially leading, but low for initially trailing waves.

A visual impression of density waves growing from initial random fluctuations of the surface density of the sheet is given in Fig 3., where snapshots of a numerical simulation of the dynamical evolution of the shearing sheet are shown (Fuchs, Dettbarn & Tsuchiya, in preparation).

**Fig. 3.** Snapshots of the growth of density waves in a numerical simulation of the dynamical evolution of the shearing sheet. The sheet was seeded initially with random noise as shown in the left panel. The right panel shows the sheet after an elapsed time of one epicyclic period. Length unit is the critical wave length  $\lambda_{\text{crit}} = 2\pi/k_{\text{crit}}$ .

### 3 The shearing sheet immersed in a live dark halo

The evolution of the distribution function of the disk stars in phase space is described by the linearized Boltzmann equation

$$\begin{aligned} \frac{\partial f_{d1}}{\partial t} + u \frac{\partial f_{d1}}{\partial x} + v \frac{\partial f_{d1}}{\partial y} - \frac{\partial \Phi_{d0} + \Phi_{h0}}{\partial x} \frac{\partial f_{d1}}{\partial u} - \frac{\partial \Phi_{d0} + \Phi_{h0}}{\partial y} \frac{\partial f_{d1}}{\partial v} \\ - \frac{\partial \Phi_{d1} + \Phi_{h1}}{\partial x} \frac{\partial f_{d0}}{\partial u} - \frac{\partial \Phi_{d1} + \Phi_{h1}}{\partial y} \frac{\partial f_{d0}}{\partial v} = 0, \end{aligned} \quad (8)$$

where  $(u, v)$  are the velocity components corresponding to the  $x$  and  $y$  coordinates, respectively. Equation (8) has been derived from the general 6-dimensional Boltzmann equation assuming delta-function like dependencies of the distribution function on the vertical  $z$  coordinate and the vertical  $w$  velocity component, respectively, and integrating the Boltzmann equation with respect to them. A perturbation Ansatz of the form

$$f_d = f_{d0} + f_{d1}, \quad \Phi_d = \Phi_{d0} + \Phi_{d1}, \quad \Phi_h = \Phi_{h0} + \Phi_{h1} \quad (9)$$

is chosen for the distribution function of the disk stars and the gravitational potentials of the disk and the halo, respectively, and the Boltzmann equation (8) has been linearized accordingly.

Similarly the linearized Boltzmann equation for the halo particles can be written as

$$\begin{aligned} & \frac{\partial f_{h1}}{\partial t} + u \frac{\partial f_{h1}}{\partial x} + v \frac{\partial f_{h1}}{\partial y} + w \frac{\partial f_{h1}}{\partial z} - \frac{\partial \Phi_{d0} + \Phi_{h0}}{\partial x} \frac{\partial f_{h1}}{\partial u} - \frac{\partial \Phi_{d0} + \Phi_{h0}}{\partial y} \frac{\partial f_{h1}}{\partial v} \\ & - \frac{\partial \Phi_{d0} + \Phi_{h0}}{\partial z} \frac{\partial f_{h1}}{\partial w} - \frac{\partial \Phi_{h1} + \Phi_{d1}}{\partial x} \frac{\partial f_{h0}}{\partial u} - \frac{\partial \Phi_{h1} + \Phi_{d1}}{\partial y} \frac{\partial f_{h0}}{\partial v} \\ & - \frac{\partial \Phi_{h1} + \Phi_{d1}}{\partial z} \frac{\partial f_{h0}}{\partial w} = 0. \end{aligned} \quad (10)$$

The choice of the dark halo model was lead by the following considerations. One of the deeper reasons for the success of the infinite shearing sheet model to describe spiral density waves realistically is the rapid convergence of the Poisson integral in self-gravitating disks (Julian & Toomre 1966). Consider, for example, the potential of a sinusoidal density perturbation

$$\Phi(x, y) = -G \int_{-\infty}^{\infty} dx' \int_{-\infty}^{\infty} dy' \frac{\Sigma_{10} \sin(kx')}{\sqrt{(x - x')^2 + (y - y')^2}}, \quad (11)$$

$$\Phi(x, y = 0) = -4G\Sigma_{10} \sin(kx) \lim_{x_L \rightarrow \infty} \frac{\text{Si}(kx_L)}{k} = -\frac{2\pi G \Sigma_{10} \sin(kx)}{k}. \quad (12)$$

The sine integral in equation (12) converges so rapidly that it reaches at  $kx_L = \frac{\pi}{2}$  already 87% of its asymptotic value. Thus the “effective range” of gravity is about only a quarter of a wave length. The shearing sheet models effectively patches of galactic disks of such size. The wave lengths of density waves are of the order of the critical wave length

$$\lambda_{\text{crit}} = \frac{2\pi}{k_{\text{crit}}} = \frac{4\pi^2 G \Sigma_0}{\kappa^2}, \quad (13)$$

where  $\kappa$  denotes the epicyclic frequency of the stellar orbits and  $\Sigma_0$  the surface density of the disk. In the solar neighbourhood in the Milky Way, for instance, the critical wave length is  $\lambda_{\text{crit}} = 5$  kpc. Thus it is reasonable to neglect over such length scales, like in the shearing sheet model, the curvature of the mean

circular orbits of the stars around the galactic center or the gradient of the surface density. The curvature of the stellar orbits due to the epicyclic motions of the stars, on the other hand, cannot be neglected and is indeed not neglected in the shearing sheet model. The radial size of an epicycle is approximately given by  $\sigma_u/\kappa$ , where  $\sigma_u$  denotes the radial velocity dispersion of the stars, and the ratio of epicycle size and critical wave length is given by

$$\frac{\sigma_u}{\kappa\lambda_{\text{crit}}} = 0.085Q \quad (14)$$

in terms of the Toomre (1964) stability parameter  $Q$  which is typically of the order of 1 to 2. Concurrent to these approximations I have assumed a dark halo which is homogeneous in its unperturbed state. Accordingly the curvature of the unperturbed orbits of the halo particles is neglected on the scales considered here and the particles are assumed to be on straight-line orbits. The equations of motion of the halo particles are the characteristics of the Boltzmann equation. In a homogeneous halo  $\dot{\mathbf{x}} = \nabla(\Phi_{d0} + \Phi_{h0}) = 0$ , and in accordance with this assumption I neglect the force terms  $\nabla\Phi_{d0}$  and  $\nabla\Phi_{h0}$  in the Boltzmann equation (10). This simplifies its solution considerably. The disadvantage of such a model is that there are no higher-order resonances of the orbits of the halo particles with the density waves as described by Weinberg (1985) or observed in the high-resolution simulations by Athanassoula (2002, 2003). However their effect was shown to be much less important than the main resonances of the particles with the density waves, which are properly described in the present model.

**Fig. 4.** Sketch of the disk and halo model.

### 3.1 Halo dynamics

The Boltzmann equation (10) can be viewed as a linear partial differential equation for the perturbation of the distribution function of the halo particles,  $f_{h1}$ , with inhomogeneities depending on the perturbations of the gravitational potentials of the disk and the halo,  $\nabla\Phi_{d1}$  and  $\nabla\Phi_{h1}$ , respectively. Thus the equation can be solved for the disk and halo inhomogeneities separately and the solutions combined afterwards by superposition. It was shown by Fuchs (2004a) that the Boltzmann equation with the inhomogeneity  $\nabla\Phi_{h1}$  describes just the Jeans instability of the dark halo. However, dark halos are thought to be dynamically hot systems and their Jeans lengths will be of the order of the size of the halos themselves. Thus this part of the solution of the Boltzmann equation (10) is uninteresting in the present context and will be not considered in the following.

More interesting is the remaining part of the Boltzmann equation (10),

$$\begin{aligned} \frac{\partial f_{h1}}{\partial t} + u \frac{\partial f_{h1}}{\partial x} + v \frac{\partial f_{h1}}{\partial y} + w \frac{\partial f_{h1}}{\partial z} \\ - \frac{\partial \Phi_{d1}}{\partial x} \frac{\partial f_{h0}}{\partial u} - \frac{\partial \Phi_{d1}}{\partial y} \frac{\partial f_{h0}}{\partial v} - \frac{\partial \Phi_{d1}}{\partial z} \frac{\partial f_{h0}}{\partial w} = 0, \end{aligned} \quad (15)$$

which describes the halo response to a perturbation in the disk. If the gravitational potential perturbation of the disk is Fourier expanded the Fourier terms have the form (cf. equation 33 of Fuchs 2001)

$$\Phi_{d\mathbf{k}_{||}} e^{i(\omega t + k_x x + k_y y) - k_{||}|z|} \quad (16)$$

with  $k_{||} = |\mathbf{k}_{||}| = \sqrt{k_x^2 + k_y^2}$ . This can be converted to Fourier coefficients of the halo potential in 3-dimensional  $\mathbf{k}$ -space as

$$\Phi_{d\mathbf{k}} = \frac{1}{2\pi} \int_{-\infty}^{\infty} dz \Phi_{d\mathbf{k}_{||}} e^{-ik_z z - k_{||}|z|} = \frac{1}{\pi} \frac{k_{||}}{k_{||}^2 + k_z^2} \Phi_{d\mathbf{k}_{||}}. \quad (17)$$

Notice that the coordinate  $y$ , which is defined in the reference system of the disk, is related to the  $y$  coordinate in the reference system of the halo due to the motion of the center of the shearing sheet as

$$y \rightarrow y - r_0 \Omega_0 t. \quad (18)$$

The further solution of the Boltzmann equation is straightforward and is described in full detail in Fuchs (2004a). The distribution function is then integrated over velocity space to obtain the Fourier coefficients  $\rho_{h\mathbf{k}}$  of the density perturbation of the dark halo. Next the gravitational potential associated with this density distribution is calculated from the Poisson equation,

$$-k^2 \Phi_{h\mathbf{k}} = 4\pi G \rho_{h\mathbf{k}}. \quad (19)$$

Since the gravitational forces in equation (8) have to be taken at the midplane  $z = 0$ , it is necessary to convert the solution of the Boltzmann equation  $\Phi_{h\mathbf{k}}$  from the representation in  $\mathbf{k}$  space to a mixed representation in  $(\mathbf{k}_{||}, z)$  space leading to two contributions

$$\begin{aligned} \Phi_{h\mathbf{k}_{||}}^{\text{nr}}(z=0) &= \int_{-\infty}^{\infty} dk_z \frac{k_{||}}{(k_{||}^2 + k_z^2)^2} \Phi_{d\mathbf{k}} \frac{4G\rho_b}{\sigma_h^2} \\ &\times \left\{ 1 + i\sqrt{\pi} \frac{k_y r_0 \Omega_0 - \omega}{\sqrt{2}k\sigma_h} \text{erf} \left( i \frac{k_y r_0 \Omega_0 - \omega}{\sqrt{2}k\sigma_h} \right) \exp - \frac{(k_y r_0 \Omega_0 - \omega)^2}{2k^2\sigma_h^2} \right\} \end{aligned} \quad (20)$$

due to halo particles not in resonance with the potential perturbation and

$$\begin{aligned} \Phi_{h\mathbf{k}_{||}}^{\text{res}}(z=0) &= - \int_{-\infty}^{\infty} dk_z \frac{k_{||}}{(k_{||}^2 + k_z^2)^2} \Phi_{d\mathbf{k}} i\sqrt{\pi} \frac{4G\rho_b}{\sigma_h^2} \\ &\times \frac{\omega - k_y r_0 \Omega_0}{\sqrt{2}k\sigma_h} \exp - \frac{(k_y r_0 \Omega_0 - \omega)^2}{2k^2\sigma_h^2} \end{aligned} \quad (21)$$

due to non-resonant halo particles.  $\rho_b$  and  $\sigma_h$  denote the mean spatial density and the velocity dispersion of the halo particles, respectively. The final result can be formally written as

$$\Phi_{h\mathbf{k}_{||}}(z=0) = \Upsilon(\omega - k_y r_0 \Omega_0, k_{||}) \Phi_{d\mathbf{k}_{||}}, \quad (22)$$

where the real and imaginary parts of  $\Upsilon$  are defined by equations (20) and (21), respectively. Thus for any given frequency there is a contribution both from the non-resonant and the resonant halo particles.

### 3.2 Disk dynamics

The halo response (22) to the perturbation in the disk has to be inserted into equation (8). Solving the Boltzmann equation (8) is greatly facilitated by the fact that its form is identical to the case of an isolated shearing sheet with the replacement

$$\Phi_{d\mathbf{k}} \rightarrow (1 + \Upsilon) \Phi_{d\mathbf{k}} \quad (23)$$

and one can use directly the results of Fuchs (2001) even though the Boltzmann equation is treated there using action and angle variables instead of the Cartesian coordinates as in equation (8). In particular the factor  $1 + \Upsilon$  is carried straightforward through to the fundamental Volterra integral equation (equation 68 of Fuchs 2001)

$$\Phi_{\mathbf{k}',\omega} = \int_{-\infty}^{k'_x} dk_x \mathcal{K}(k_x, k'_x) (1 + \Upsilon(k_x, k'_x, \omega)) \Phi_{k_x, k'_y, \omega} + r_{\mathbf{k}',\omega}, \quad (24)$$

where the kernel  $\mathcal{K}$  is given by equation (67) of Fuchs (2001).  $r_{\mathbf{k}'}$  describes an inhomogeneity of equation (24) related to an initial non-equilibrium state of the shearing sheet. Equation (24) is separating in the circumferential wave number  $k'_y$ . In equation (24) the wave numbers are expressed in units of the critical wave number  $k_{\text{crit}}$ . This implies that the Volterra equation describing a shearing sheet embedded in a rigid halo potential is formally the same as that of an isolated shearing sheet, because in this case  $\Upsilon = 0$  and the halo mass affects only the numerical values of the critical wave number  $k_{\text{crit}}$  and the stability parameter  $Q$ . It is advantageous to consider equation (24) transformed back from frequency to time domain. Splitting off the  $\omega$ -dependent term  $\exp i\omega \frac{k_x - k'_x}{2Ak'_y}$  from the kernel and making use of the convolution theorem of the Fourier transform of products of two functions leads to

$$\begin{aligned} \Phi_{\mathbf{k}',t} = & \int_{-\infty}^{k'_x} dk_x \tilde{\mathcal{K}}(k_x, k'_x) \left\{ \int_0^\infty dt' \Phi_{k_x, k'_y, t'} \delta \left( t - t' + \frac{k_x - k'_x}{2Ak'_y} \right) \right. \\ & \left. + \int_0^\infty dt' \Phi_{k_x, k'_y, t'} \mathcal{F} \left( \Upsilon(k_x, k'_y, \omega) e^{i\omega \frac{k_x - k'_x}{2Ak'_y}} \right) \right\}_{t-t'} + r_{\mathbf{k}',t}, \end{aligned} \quad (25)$$

where the operator  $\mathcal{F}$  denotes the Fourier transform from  $\omega$  to time domain. In equation (33) I have assumed an initial perturbation of the disk at time  $t = 0$  so that  $\Phi_{k_x, k'_y, t' < 0} = 0$ . The Fourier transform  $\mathcal{F}$  is given by equation (34) of Fuchs (2004a). If this is inserted into equation (25) it takes the form

$$\begin{aligned} \Phi_{k', t} = & \int_{-\infty}^{k'_x} dk_x \tilde{\mathcal{K}}(k_x, k'_x) \{ \Phi_{k_x, k'_y, t + \frac{k_x - k'_x}{2A k'_y}} \\ & + \int_0^{t + \frac{k_x - k'_x}{2A k'_y}} dt' \Phi_{k_x, k'_y, t'} \mathcal{F} \left( \Upsilon(k_x, k'_y, \omega) e^{i\omega \frac{k_x - k'_x}{2A k'_y}} \right) \}_{t-t'} \} + r_{k', t}. \end{aligned} \quad (26)$$

Equation (26) can be integrated numerically with very modest numerical effort. In Fig. 5 I illustrate the response of the shearing sheet now embedded in a live halo to an initial sinusoidal perturbation of unit amplitude. For this purpose I use the inhomogeneity term of the Volterra equation

$$r_{k', \omega} = \int_{-\infty}^{k'_x} dk_x \mathcal{L}(k_x, k'_x) f_{k_x, k'_y}(0) \quad (27)$$

derived in Fuchs (2001) with  $f_{k_x, k'_y}(0) \propto \delta(k_x - k_x^{\text{in}})$ . The response of the shearing sheet to this initial impulse is a swing amplification event as described in section (2). The radial wave number  $k_x$  evolves as

$$k_x = k_x^{\text{in}} + 2A k'_y t, \quad (28)$$

while the circumferential wave number  $k'_y$  is constant, which means that the wave crests swing around from leading to trailing orientation during the amplification phase. Around  $t = 6$  the amplitudes become negative which indicates that the swing amplified density wave is also oscillating. As can be seen from Fig. 5 comparing the evolution of shearing sheets embedded either in a rigid halo potential or a live halo this characteristic behaviour of the density wave is not changed by the responsive halo, but the maximum growth factor of the amplitude of the wave is enhanced by a surprisingly large amount.

**Fig. 5.** Swing amplified density wave in the shearing sheet. The upper diagram shows the evolution in a shearing sheet embedded in a static halo potential triggered by an impulse with unit amplitude and wave vector  $\mathbf{k}^{\text{in}} = (-2, 0.5)k_{\text{crit}}$ . Time is given in units of  $(2A k_y^{\text{in}} / k_{\text{crit}})^{-1}$ . The middle diagram shows the evolution of a shearing sheet embedded in a live dark halo triggered by the same impulse. The lower diagram shows the difference. The model parameters are  $A/\Omega_0 = 0.5$ ,  $Q = 1.4$ ,  $\sigma_d : \sigma_h = 1 : 5$ ,  $G \rho_b / \kappa^2 = 0.01$ , and  $r_0 \Omega_0 : \sigma_d = 220 : 44$ .

The enhanced maximum growth factor of swing amplified density waves due to a responsive halo seems to be the equivalent of the enhanced growth of

bars of stellar disks embedded in live dark halos seen in the numerical simulations. However, the interaction of the shearing sheet and the surrounding halo is not only mediated by the resonant halo particles, but the non-resonant halo particles play an important role as well. The amplification of density waves depends critically on the Toomre stability parameter  $Q$ . This is illustrated in Fig. 6 where the response of the shearing sheet to the same initial impulse as in the previous example is shown, but assuming a stability parameter of  $Q = 2$ . As can be seen in Fig. 6 there is neither effective amplification of density waves in a shearing sheet in a rigid halo potential or in a shearing sheet embedded in a live dark halo.

**Fig. 6.** Same as in Fig. 5, but adopting  $Q = 2$ .

#### 4 Wakes in dark matter halos

The perturbations of the gravitational potential and the surface density of the shearing sheet have their counterparts in the dark matter halo. From equation (19) one obtains

$$\rho_{h\mathbf{k}||}(z, \omega) = - \int_{-\infty}^{\infty} dk_z \frac{k^2}{4\pi G} \Phi_{h\mathbf{k}} e^{ik_z z}, \quad (29)$$

where the Fourier coefficients  $\Phi_{h\mathbf{k}}$  derived in section (3.1) have to be inserted,

$$\begin{aligned} \rho_{h\mathbf{k}||}(z, \omega) = & - \int_{-\infty}^{\infty} dk_z \frac{k_{||}}{k_{||}^2 + k_z^2} \Phi_{d\mathbf{k}||} \frac{\rho_b}{\pi \sigma_h^2} e^{ik_z z} \\ & \times \left\{ 1 + i\sqrt{\pi} \frac{k_y r_0 \Omega_0 - \omega}{\sqrt{2} k \sigma_h} \left( 1 + \text{erf} \left( i \frac{k_y r_0 \Omega_0 - \omega}{\sqrt{2} k \sigma_h} \right) \right) \exp - \frac{(k_y r_0 \Omega_0 - \omega)^2}{2 k^2 \sigma_h^2} \right\}. \end{aligned} \quad (30)$$

Equation (30) can be Fourier transformed back from frequency to time domain in the same way as equation (32) of Fuchs (2004a) was Fourier transformed back to time domain by a convolution of  $\Phi_{d\mathbf{k}||}(t')$  with the Fourier transform of the remaining terms under the integral with respect to  $k_z$ . To these terms the operator

$$\int_{-\infty}^{\infty} d\omega e^{i(\omega - k_y r_0 \Omega_0)t} \dots \quad (31)$$

is applied and the integral over  $\omega$  is evaluated with the help of formulae (6.317) and (3.952) of Gradshteyn & Ryzhik (2000) leading effectively to expression (34) of Fuchs (2004a) with  $t - t' + \frac{k_x - k'_x}{2 A k'_y}$  replaced by  $t - t'$  only. The integral over  $k_z$  can be then calculated using formulae (3.723) and (3.896) of Gradshteyn & Ryzhik (2000) with the result

$$\begin{aligned} \rho_{h\mathbf{k}||}(z, t) = & -\frac{\rho_b}{\sigma_h^2} \{ 2\pi \Phi_{d\mathbf{k}||}(t) e^{-k_{||}|z|} \\ & + \sqrt{8\pi} \sigma_h k_{||} \int_{-\infty}^t dt' \Phi_{d\mathbf{k}||}(t') e^{-\frac{1}{2}\sigma_h^2 k_{||}^2 (t-t')^2} e^{ik_y r_0 \Omega_0 (t-t')} e^{-\frac{z^2}{2\sigma_h^2 (t-t')^2}} \} , \end{aligned} \quad (32)$$

and finally I convert the potential perturbation of the disk to the perturbation of its surface density with the relation  $k_{||}\Phi_{d\mathbf{k}||} = -2\pi G \Sigma_{d\mathbf{k}||}$  (cf. Fuchs 2001) and obtain

$$\begin{aligned} \frac{\rho_{h\mathbf{k}||}}{\rho_b} = & \frac{2\pi G \Sigma_d}{\sigma_h^2} \{ \frac{2\pi}{k_{||}} \frac{\Sigma_{d\mathbf{k}||}(t)}{\Sigma_d} e^{-k_{||}|z|} \\ & + \sqrt{8\pi} \sigma_h \int_{-\infty}^t dt' \frac{\Sigma_{d\mathbf{k}||}(t')}{\Sigma_d} e^{-\frac{1}{2}\sigma_h^2 k_{||}^2 (t-t')^2} e^{ik_y r_0 \Omega_0 (t-t')} e^{-\frac{z^2}{2\sigma_h^2 (t-t')^2}} \} . \end{aligned} \quad (33)$$

The time integral in equation (33) has been calculated numerically. At the time of maximal amplification of the density wave I find, adopting the same parameters used to calculate Fig. 5,  $\rho_{h\mathbf{k}}/\rho_b|_{\text{peak}} = 0.6 \Sigma_{d\mathbf{k}}/\Sigma_0|_{\text{peak}}$ . Fig. 7 shows the vertical profile of the density perturbation of the dark halo according to equation (33). As can be seen from Fig. 7 the profile indicates a density enhancement of dark halo matter close above the density wave crest. At larger distances above the midplane there is a density deficit above the density wave crest, which means that the cloud of dark matter particles is lagging behind like a trail of smoke.

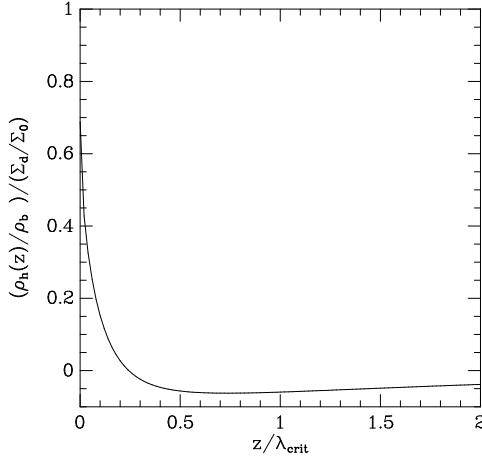


**Fig. 7.** Vertical profile of the density perturbation in the dark halo induced by a density wave in the sheet, which is at maximal amplification, exactly above the density wave crest. The relative density contrast  $\rho_{h\mathbf{k}}/\rho_b|_{\text{peak}}$  is given in terms of the relative density contrast of the surface density of the sheet  $\Sigma_{d\mathbf{k}}/\Sigma_0|_{\text{peak}}$ .

The existence of wakes in dark matter halos might have quite practical implications. For instance the bar in the Milky Way focusses dark matter particles dynamically into some regions in phase space and depopulates others, which may very well affect the flux of dark matter particles through detectors on Earth. Such features have been observed as ‘star streams’ in velocity space among the stars in the solar neighbourhood (Dehnen 2000, Mühlbauer & Dehnen 2003). These stars are, of course, stars members of the Milky Way disk, but similar effects are to be expected among halo objects.

## References

1. E. Athanassoula: *Astroph. J.*, **569**, L83 (2002)
2. E. Athanassoula: *Mon. Not. R. Astron. Soc.*, **341**, 1179 (2003)
3. V.P. Debattista, J. A. Sellwood: *Astroph. J.*, **543**, 704 (2000)
4. W. Dehnen: *Astron. J.*, **119**, 800 (2000)
5. B. Fuchs: Recurrent swing amplification induced by nonlinear amplitude effects. In: *Dynamics of disc galaxies* ed by B. Sundelius (Göteborgs Univ. and Chalmers Univ. of Tech., Göteborg 1991) pp 359–363
6. B. Fuchs: *Astron. Astroph.*, **368**, 107 (2001)
7. B. Fuchs: *Astron. Astroph.*, **419**, 941 (2004a)
8. B. Fuchs: *Astron. Astroph.*, submitted (2004b)
9. P. Goldreich, D. Lynden–Bell: *Mon. Not. R. Astron. Soc.*, **130**, 125 (1965)
10. Gradshteyn, I.S., Ryzhik, I.M.: *Table of Integrals, Series, and Products*, 6th edn (Academic Press, New York 2000)
11. W.H. Julian, A. Toomre: *Astroph. J.*, **146**, 810 (1966)
12. A. Kalnajs: 1971, *Astroph. J.*, **166**, 275 (1971)
13. G. Mühlbauer, W. Dehnen: *Astron. Astroph.*, **401**, 975 (2003)
14. J.P. Ostriker, P.J.E. Peebles: *Astroph. J.*, **186**, 467 (1973)
15. A. Toomre: *Astroph. J.*, **139**, 1217 (1964)
16. A. Toomre: *Ann. Rev. Astron. Astroph.*, **15**, 437 (1977)
17. A. Toomre: What amplifies the spirals? In: *The Structure and Evolution of Normal Galaxies* ed by S.M. Fall, D. Lynden–Bell (Cambridge Univ. Press, Cambridge 1981) pp 111–136
18. M.D. Weinberg: *Mon. Not. R. Astron. Soc.*, **213**, 451 (1985)

This figure "BFDark2004f1.jpg" is available in "jpg" format from:

<http://arxiv.org/ps/astro-ph/0501050v1>

This figure "BFDark2004f2.jpg" is available in "jpg" format from:

<http://arxiv.org/ps/astro-ph/0501050v1>

This figure "BFDark2004f3.jpg" is available in "jpg" format from:

<http://arxiv.org/ps/astro-ph/0501050v1>

This figure "BFDark2004f4.jpg" is available in "jpg" format from:

<http://arxiv.org/ps/astro-ph/0501050v1>

This figure "BFDark2004f5.jpg" is available in "jpg" format from:

<http://arxiv.org/ps/astro-ph/0501050v1>

This figure "BFDark2004f6.jpg" is available in "jpg" format from:

<http://arxiv.org/ps/astro-ph/0501050v1>